Title	Influence of doping on the photoactive properties of magnetron-sputtered titania coatings: Experimental and theoretical study
Authors(s)	McDonnell, Kevin, English, Niall J., Rahman, Mahfujur, et al.
Publication date	2012-09
Publication information	McDonnell, Kevin, Niall J. English, Mahfujur Rahman, and et al. "Influence of Doping on the Photoactive Properties of Magnetron-Sputtered Titania Coatings: Experimental and Theoretical Study" 86, no. 11 (September, 2012).
Publisher	American Physical Society
Item record/more information	http://hdl.handle.net/10197/4676
Publisher's version (DOI)	10.1103/PhysRevB.86.115306

Influence of doping on the photoactive properties of magnetron-sputtered titania coatings: Experimental and theoretical study

Kevin A. McDonnell,[1,2] Niall J. English,[2,*] Mahfujur Rahman,[2] and Denis P. Dowling[1,2]

[1]*School of Mechanical and Materials Engineering, University College Dublin, Belfield, Dublin 4, Ireland*

[2]*The SEC Strategic Research Cluster and the Centre for Synthesis and Chemical Biology, School of Chemical and Bioprocess Engineering, University College Dublin, Belfield, Dublin 4, Ireland*

Titanium dioxide (TiO_2) thin films, doped with chromium (Cr) and codoped with chromium-carbon (Cr, C) and chromium-nitrogen (Cr, N) of various concentrations, were deposited using magnetron sputtering. Postdeposition thermal treatments were carried out at $450\,°C$ for 5 h to change the as-deposited amorphous coatings to their crystalline form. The crystalline phase was found to be dependent on the amount and type of dopant present. Ultraviolet-visible (UV-Vis) absorption data and band gap energies calculated by spectroscopic ellipsometry showed that, on increasing Cr concentration, a shift of the absorption edge towards visible light and a reduction of the band gap occurred. This was further improved by codoping of Cr with either N or C, with the latter case exhibiting more photo-activity towards visible light. In addition, hybrid density functional theory (DFT) calculations were performed for Cr-, N-, and C-monodoping, together with Cr-C and Cr-N codoping, in both rutile and anatase phases of crystalline titania. Using this method, absorption coefficients and band gaps were determined to explore photo-activity. Very good, semiquantitative agreement was found between the DFT and experimental approaches for these quantities, underlining the key role of state-of-the-art quantum calculations in interpreting and guiding experimental studies of doping in metal oxides.

PACS number(s): 78.20.−e

I. INTRODUCTION

Crystalline TiO_2 coatings have been investigated extensively for application in solar cells, self-cleaning surfaces, and water pollution control, due to their good photocatalytic behavior,[1] relative cheapness, resistance to corrosion, and environmentally friendly, nontoxic nature.[2] However, the widespread technological use of TiO_2 is hindered by its low utilization of light in the visible range due to its wide band gap of 3.2 eV, in its most photo-active form, anatase. Doping in titania with metals and nonmetals[3–10] using a variety of methods, such as sputtering,[11–13] sol-gel approaches,[14] cathodic arc methods,[15] and ion implantation,[16] has been reported widely.

Recently, Asahi *et al*.[3] reported that N-doped TiO_2 leads to a significant improvement vis-à-vis pure TiO_2 for optical absorption and photocatalytic activity. C-doped TiO_2 has experienced particular attention since Sakthivel *et al*.[17] reported that C-doped powder is roughly five times more active than its N-doped analogue in the light-driven degradation of 4-chlorophenol ($\lambda \geqslant 455$ nm). Other experiments have also reported the red shift of the optical absorption edge.[18,19] The nature of C-induced changes to the TiO_2 electronic band structure is controversial. Both band gap narrowing[20] and the formation of localized midgap states[21] have been proposed to account for the red shift of the optical absorption edge. The codoping of TiO_2 with C and N by Chen *et al*.[22] using the sol-gel technique was also found to further enhance the photo-activity of TiO_2 towards visible light. Given the lesser prevalence of experimental or theoretical studies of nonmetal/metal codoping in titania, the study of Gai *et al*.[23] outlines the attractive prospect of modulating the band edges of TiO_2 to extend titania's optical absorption edge to the visible light region via codoping by suitable nonmetal and metal elements—passivated codoping. In a similar vein,

Zhu *et al*.[24] have recently employed both experimental and DFT techniques to gauge noncompensated anion-cation codoping in titania, in conjunction with experiment; here, *n-p* codoping of Cr and N in anatase was found to result in improved photocatalytic properties. Experimentally, Zhu *et al*.,[24] amongst others mentioned previously, have used a wet chemistry method of creating their coatings. In comparison to sputtered coatings, these tend to be less durable and inhomogeneous along with being extremely susceptible to shrinkage on thermal treatment. Comparisons in the literature between physically and chemically synthesized TiO_2 have been shown to indicate a higher visible light absorption for the physically deposited coating,[25] and hence this route was followed in this study via magnetron sputtering, building on our recent work in this area.[26,27]

In recent years, the increasing availability of computing power and maturity of quantum electronic structure methods has led to the application of density functional theory (DFT) and higher-order quantum chemical simulation methods to determine the electronic structure of metal oxides, such as titania. In particular, its use as a design tool to predict the electronic structure of potential photocatalytic materials and to filter the most promising ones prior to experiment is clearly attractive. However, the accurate characterization of the electronic structure of titania by DFT remains elusive, although there have been a number of studies devoted to this.[28] The band gaps of transition metal oxides are underestimated routinely by the generalized gradient approximation (GGA) of DFT due to the less accurate description of strong Coulomb and exchange interactions between electrons in the same *d* shell. Our previous DFT studies of mono- and codoping in titania[29,30] have frequently made use of this design principle in an effort to gauge and tailor the electronic structure of doped titania, with particular emphasis on metal and non-metal elements. These theoretical approaches from DFT and insights into possible

TABLE I. Results of the Tauc plot fitting for both ellipsometry and Ultraviolet-visible (UV-vis) measurements. The energy of the fundamental band gap E_{fun} and the energy of the excitation related to doping E_{dop} vs Cr concentration in TiO_2.

Applied Cr target current (A)	at% Cr	Ellipsometry		UV-vis		Crystallite phase
		$E_{\text{fun}} +/- 0.1$(eV)	$E_{\text{dop}} +/- 0.1$(eV)	$E_{\text{fun}} +/- 0.1$(eV)	$E_{\text{dop}} +/- 0.1$(eV)	
0.00	0.0	3.40		3.26		Anatase
0.20	0.6	3.38	3.21	3.29	3.08	Anatase
0.30	1.8	3.36	2.64	3.26	3.14	Anatase
0.35	2.3	3.16	2.55	3.32	3.05	Rutile
0.40	2.5	3.13	2.42	3.23	2.83	Rutile
0.50	2.9	3.08	2.34	3.24	2.64	Rutile
1.00	5.0	2.91	2.23	2.91	2.11	Amorphous

doping-mediated enhancements in photo-activity, and certainly the detailed investigation of changes in electronic structure, have led us to where we believe DFT has matured to the point of being able to offer much to experiment in terms of interpreting results and planning experiments for particular promising materials—*de facto* pre-experiment *in silico* design for screening. Bearing this goal in mind, in this paper, we have combined magnetron sputtering and state-of-the-art hybrid DFT calculations, using the PBEsol functional to give essentially exact geometry (with deviations within around 0.25% from experiment) to gauge the doping of chromium, a promising transition metal candidate, into the TiO_2 lattice along with carbon and nitrogen codopants (for both anatase and rutile forms, *in silico* and postannealing). In DFT, the cell and structural parameters were calculated, along with band gaps and optical absorption spectra, offering insight into and complementing the experimental results.

II. METHODOLOGY

A. Experimental methods

Undoped and doped TiO_2 coatings were deposited on titanium (Ti), silicon (Si), and glass substrates using a Teer Coating UDP450 magnetron sputtering machine with a closed field arrangement. The substrates were cleaned ultrasonically in methanol and acetone for 5 min each prior to being cleaned in an Argon (Ar) (BOC Gases purity 99.998%) plasma at a deposition pressure of 2×10^{-3} mbar with a bias voltage of -400 V for 20 min. The coatings were deposited at a pressure of 4×10^{-3} mbar with a bias of -50 V. The samples were positioned at a distance of 100 mm from the targets and rotated at 2 rpm. Two active targets, Ti and Cr (Teer Coatings Ltd purity <99.5%) with dimensions of $300 \times 100 \times 2$ mm and two dummy targets were used to complete the closed magnetic field. The Ti target current was held constant at 2 A, and stoichiometric TiO_2 was formed by controlling the oxygen flow rate with a Reactaflo reactive sputtering controller while monitoring the Ti peak. To study the effect of the concentration of Cr dopant on TiO_2, the current on the target was adjusted between 0.1 and 1.0 A. Nonmetallic dopants C and N were also codoped by introducing trace levels of CO_2 (1–4 sccm) and N_2 (0.5 to 2 sccm), respectively, into the deposition chamber. Post-thermal treatments were required to convert the as-deposited amorphous coatings into their crystalline form. Heat treatments were conducted in vacuum in a tube furnace where samples were heated at a rate of 2 °C/min up to 450 °C and maintained at this temperature for 5 h before being cooled slowly to room temperature.

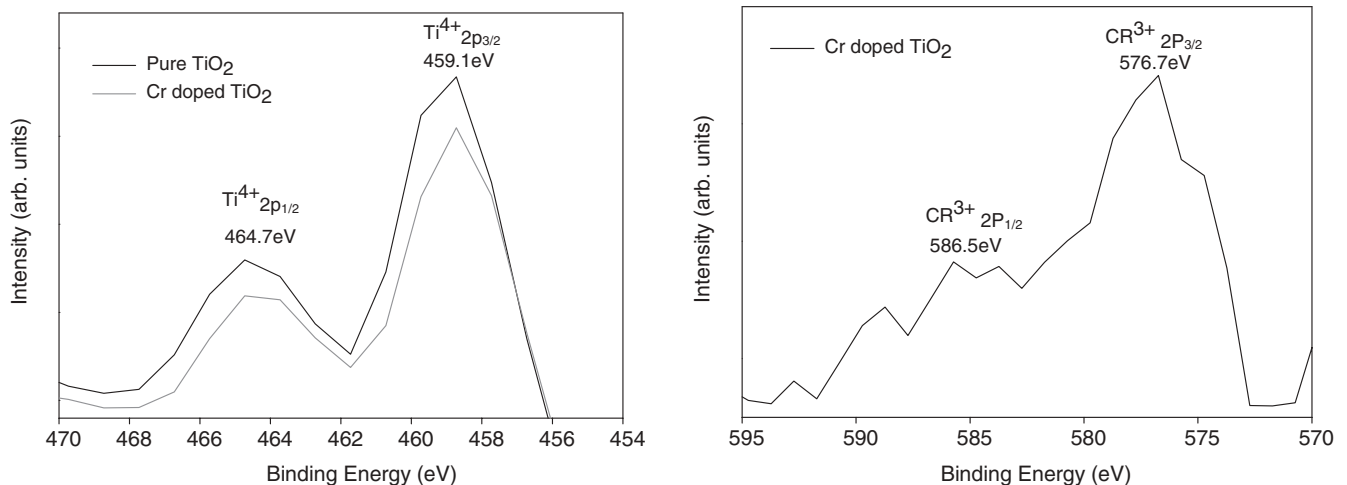Coating thickness and band gaps were measured using a variable angle M-2000 ellipsometer from J. A. Woollam

FIG. 1. XPS profiles of the binding energies for TiO_2 (left) and Cr^{3+} (right).
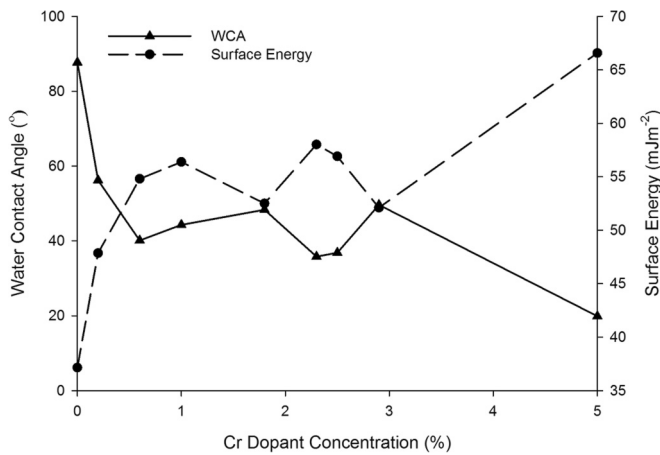
FIG. 2. Change in water contact angle (WCA) and surface energy values for various concentrations of Cr-doped TiO_2.

Co using an FLS 300 75W Xenon arc lamp operating within a wavelength range of 270–1700 nm. Measurements at an incident angle of $65°$, $70°$, and $75°$ at three different points on the sample were made. A three-layer model using a Tauc–Lorentz top layer was used to model the ellipsometry data and obtain the thickness and optical constants.[31] The band gap was calculated by plotting a Tauc plot of absorption energy against energy and taking a tangent of the slope and noting the intercept on the ordinate axis.[32]

Chemical composition and bonding information was measured using x-ray photoelectron spectroscopy (XPS) analysis of the samples using a Kratos AXIS 165 spectrometer with a monochromatic x-ray source (Al Kα 1486.58 eV). Measurements were taken with a $90°$ takeoff angle at the surface and at depth by sputtering with an Ar ion beam of 2 keV for 2 min. The crystallinity of the coatings was examined using a Siemens D500 diffractometer (XRD). The system was operated using a voltage of 40 kV and a current of 30 mA

using Cu Kα radiation at a wavelength of 0.1542 nm. Light absorption was measured using an Analytik Jena Specord 210 Uv-Vis spectrometer in transmission mode.

The water contact angle and surface energy measurements were measured using a sessile drop technique, by means of a Dataphysics Instruments OCA 20. Both measurements were carried out at room temperature with surface energy being calculated from three liquids, water, diodemethane, and ethylene glycol, using the Owens, Wendt, Rabel and Kaelbe (OWRK) method. A minimum of three measurements for each liquid was taken with a standard deviation of less than $2°$ from the mean being observed.

The morphology and surface roughness of the sample surface was examined using a Wyko NT1100 optical profilometer operating in vertical scanning interferometry (VSI) mode with a $×50$ lens. The surfaces were also examined in more detail using a CP-II (Veeco) atomic force microscope (AFM). The AFM images were recorded in noncontact mode with silicon (phosphorous doped) cantilevers (Veeco, nominal spring constant = 40 N/m, tip radius < 10 nm)

The photocurrent density, which is proportional to the rate of water splitting reaction to hydrogen and oxygen on the photocathode and photoanode, respectively, was used as a means of assessing water splitting in a photoelectrochemical (PEC) cell.[33] The measurements of photocurrent were carried out using a custom-made photoelectrochemical (PEC) cell, a Gamry G300 potentiostat, and a Newport 450W (xenon arc lamp) solar simulator. The PEC cell consists of three electrodes: a working electrode (TiO_2 coating), a counter platinum electrode, and a reference electrode immersed in an electrolyte aqueous solution of 1 M NaOH.

B. Computational methods

Three-dimensional periodic spin-polarized density functional theory (DFT) calculations were performed using the Heyd–Scuseria–Ernzerhof (HSE06) hybrid functional,[34–36] as
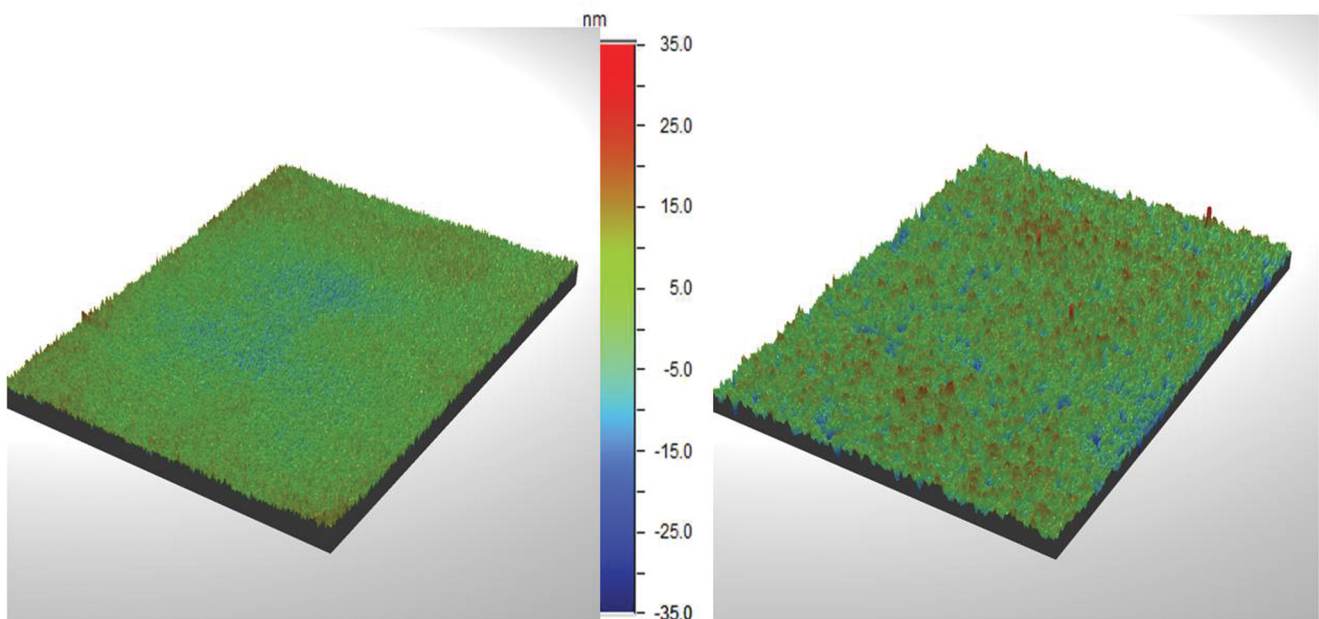

FIG. 3. (Color online) Profilometry image of the surface roughness of pure TiO_2 (left); and 5 at% Cr-doped titania (right).
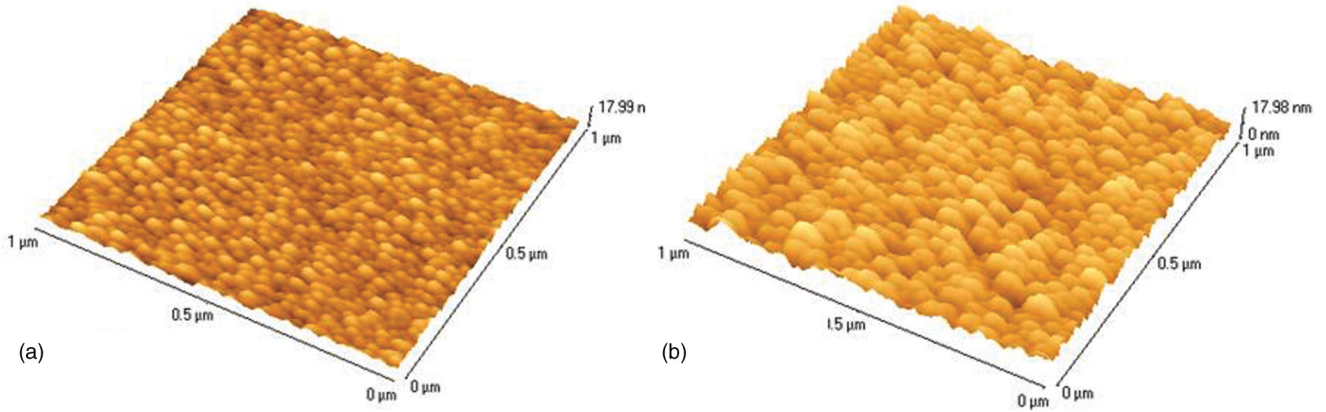
FIG. 4. (Color online) AFM topographical morphology of (a) undoped and (b) 5 at% Cr-doped sputtered-deposited TiO_2 coating.

implemented in the Vienna *ab initio* Simulation Package (VASP) code (v5.2.11),[37,38] using projector augmented wave (PAW) pseudopotentials. The exchange-correlation potential is divided into short- and long-range parts, and Hartree–Fock (HF) exchange correlation is mixed with Perdew–Burke–Ernzerhof (PBEsol) exchange correlation, as adjusted for solids,[39] in the short-range part. Here, PBEsol was used due to its superior geometry prediction vis-à-vis PBE exchange correlation in solids,[39,40] leading to more accurate Born–Oppenheimer forces acting on the electronic wave functions, providing the best possible estimation of electronic properties. To avoid the expensive calculation of long-range HF exchange, this term is replaced by long-range PBEsol exchange, as shown in following equation:

$$E_{xc}^{HSE} = \tfrac{1}{4} E_x^{HF,sr,\mu} + \tfrac{3}{4} E_x^{PBE,sr,\mu} + E_x^{PBEsol,lr,\mu} + E_c^{PBEsol},$$
$$(1)$$

where sr and lr refer to the short- and long-range parts of the respective exchange interactions. Control of the range separation may be achieved by varying the Coulomb kernel, typically between 0.2 and 0.3 A^{-1}. We have used $\mu = 0.2$ A^{-1} for HSE06; the exact exchange contribution of 25% [cf. Eq. (1)] was suggested originally by Becke[41,42] by fits to atomization energy data of a large number of molecular species and is reasonably applicable in hybrid-DFT. Although contributions other than 25% can yield more accurate intrinsic band gaps (i.e. determined from electronic structure), for instance, for specific materials, this contribution is still widely applicable and relevant for a wide range of materials. In any event, this choice of parameters for HSE06-PBEsol is identical to the recent work of Schimka *et al.*,[43] who have found that this works well for a range of solids.

Here, 48-atom ($2 \times 2 \times 1$) anatase and ($2 \times 2 \times 2$) rutile supercells were constructed. Single titanium (Ti) and oxygen (O) atoms were replaced by single chromium (Cr) and X (nitrogen (N), carbon (C)) atoms, respectively, to construct the substitutional monodoped supercells and the codoped supercells in the fashion of first nearest neighbor (1 nn), i.e. with codopants adjacent. This was found to lead to lowest-energy structures as compared to greater distances between the codopants, in line with previous findings.[29] The atomic concentration of impurity was 2.08 at.% for monodoping and

about 4.15 at% for the Cr/N and Cr/C codoping, which is comparable to the concentrations investigated experimentally. The electronic wave function was expanded in plane waves up to a cutoff energy of 400 eV, and a Monkhorst–Pack k-point mesh[44] of $2 \times 2 \times 2$ was used for geometry optimization and electronic structure calculations. Both the atomic positions and cell parameters were optimized until residual forces were below 0.01 eV/A. The optimized lattice parameters for both rutile and anatase were found to be within around 0.25% agreement with experimental values.[45,46]

III. RESULTS AND DISCUSSION

A. Monodoping

X-ray photoelectron spectroscopy results for the Cr-doped samples indicate that, with an increased applied current to the Cr target, an increase in Cr-dopant concentration was observed, as shown in Table I. The thermally treated coatings showed a higher Cr concentration at the surface than that of their amorphous as-deposited counterparts. A likely explanation for this is that, on thermal treatment, the Cr atoms may have obtained enough energy to migrate through the lattice
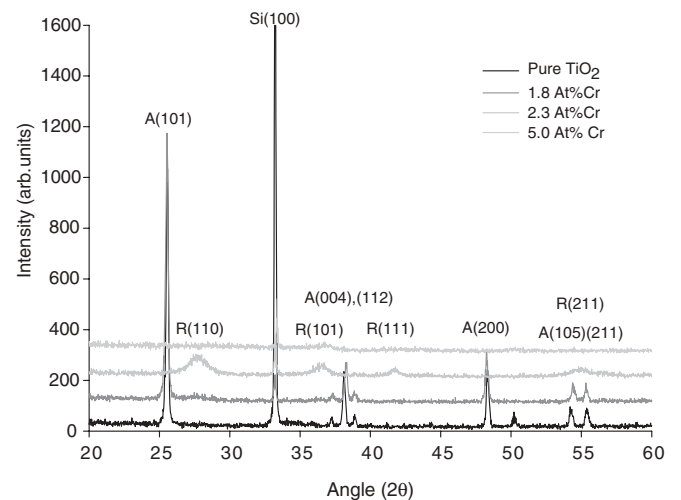

FIG. 5. XRD spectra for selected thermally treated Cr-doped TiO_2 films with different dopant concentration.
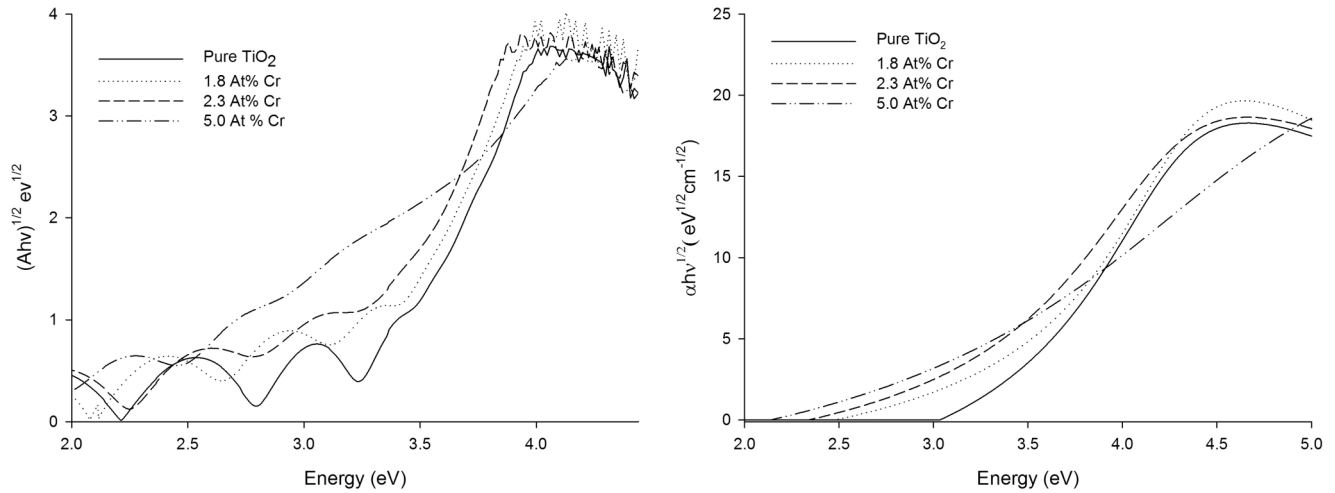
FIG. 6. Tauc plots of undoped and doped TiO$_2$ with different Cr-dopant concentration measured using UV-vis (left) and ellipsometry (right).

to the surface through the oxygen vacancies by a vacancy diffusion mechanism.[47] Further analysis of the XPS spectra of the samples in Fig. 1 shows two peaks at 459.1 and 464.7 eV for pure TiO$_2$, which corresponds to Ti^{4+}2$p_{3/2}$ and Ti^{4+}2$p_{1/2}$ electronic levels. Cr-doped samples displayed peaks at 576.7 and 586.5 eV, which are assigned to the 2$p_{3/2}$ and 2$p_{1/2}$ orbitals of the Cr^{3+} species, respectively.[13] This indicates that Cr atoms are present in the titania coating. No noticeable shifts in the titanium peaks for the chromium-doped samples were seen. The absence of a peak shift in this study may be attributed to the low atomic concentrations of 5 at% and below being dealt with. Dholam *et al.* showed a 0.3-eV shift with a much larger 9 at% Cr-dopant concentration.[12]

Coating thickness was measured using spectroscopic ellipsometry and was found to be between 300 and 360 nm for all the Cr-monodoped coatings measured. A slight increase in thickness was seen with increased Cr concentration, resulting from a greater flux of chromium ions being ejected off the target as the current was increased.

Figure 2 shows plots of water contact angle and surface energy as the chromium concentration is increased. As the

Cr concentration was increased, the surface energy increased, coinciding with a subsequent decrease in water contact angle. Changes in contact angle and surface energy can occur due to a wide range of contributing factors, with surface roughness and oxygen being some of the most prevalent. A small increase in surface roughness with increasing dopant concentration was observed (cf. Fig. 3). This accounts to some degree for the drop in contact angle along with possible changes in surface chemistry.

Figure 3 shows profilometry images for pure TiO$_2$ and Cr-doped TiO$_2$ measured in vertical scanning interferometry (VSI) mode using a 50$\times$ lens. A clear difference in the surface roughness was noted between the two, with the pure TiO$_2$ having an average roughness R_a of 4 nm, while that of the Cr-doped sample was 6 nm. The root mean squared roughness R_q was also significantly higher for the Cr-doped sample, 7 nm compared to 5 nm for pure TiO$_2$.

Figure 4 depicts AFM images for doped and Cr-doped TiO$_2$. The average roughness of the coating is 50% higher for the Cr-doped sample when compared to its undoped counterpart. The average roughness R_a for undoped TiO$_2$ is 1.2 nm, while
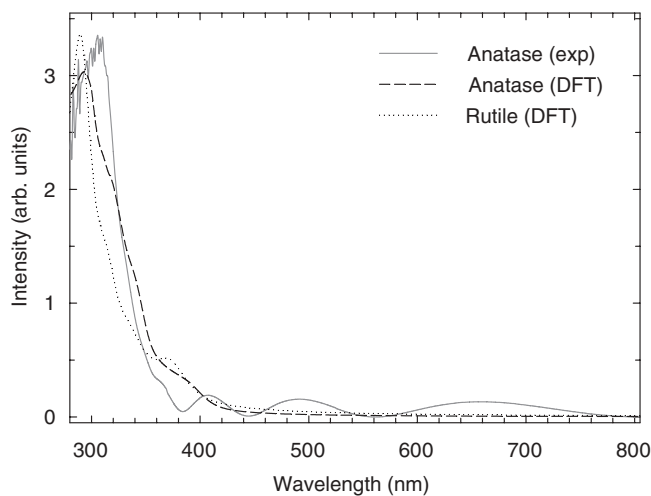

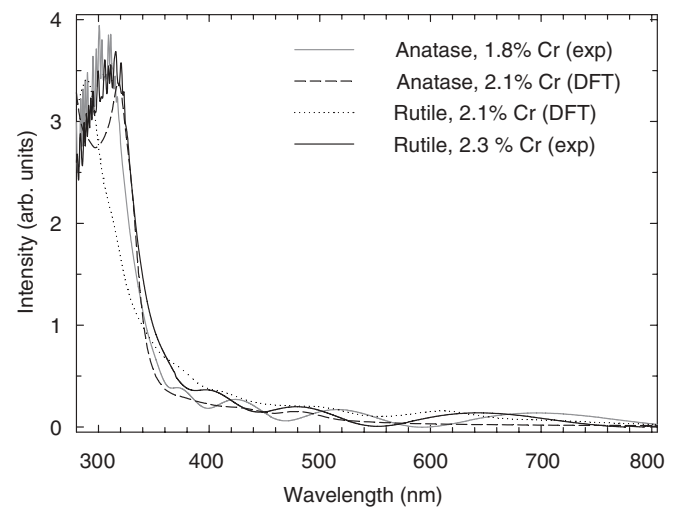FIG. 7. Absorption spectra from experiment and DFT for pure titania.

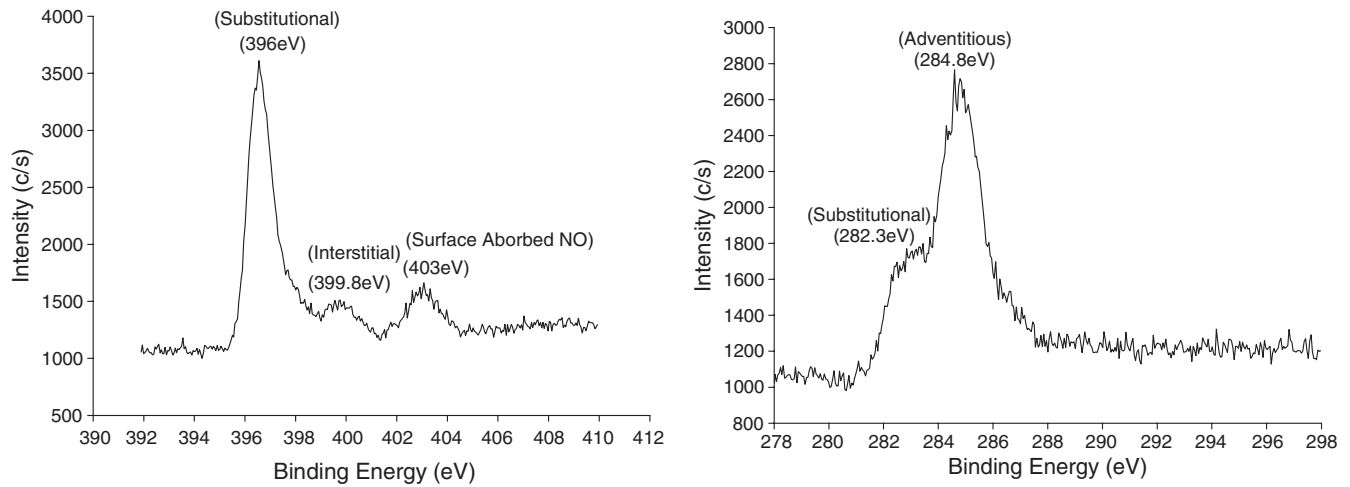FIG. 8. Absorption spectra from experiment and DFT for Cr-doped titania.

FIG. 9. XPS of N-doped TiO_2 indicating both substitutional and interstitial doped atoms (left) and substitutionally doped C atoms (right).

that of Cr doped is 1.8 nm. The resulting fractal dimension also increases from 2.67 to 2.75.

Figure 5 depicts XRD spectra of the annealed Cr-doped TiO_2 films of varying concentrations deposited onto Si substrates. The as-deposited coatings deposited showed an amorphous structure exhibiting no peaks. No characteristic peaks of chromium oxides (Cr_2O_3 and CrO_2) were found in the XRD spectra, implying either pure chromium was doped into the crystalline structure of TiO_2, or else these oxides were highly dispersed or very small. Cr^{3+} metal ions have an effective diameter similar to that of Ti^{4+} ion; therefore, substitution of the Ti atom with a Cr atom may facilitate substitution with little change to the crystalline structure.

The crystallite size for the anatase-101 peak was calculated from the Debye–Scherrer equation for coatings, which exhibited an anatase form. A restriction in the crystallization of the TiO_2 was observed as the Cr concentration was increased, resulting in smaller anatase crystallites. The crystallite phase of the Cr-doped TiO_2 was also seen to be dependent on the amount of dopant present in the coatings. The anatase phase was seen below 2 at % Cr, with rutile above this to concentrations of around 4 at % Cr. An amorphous structure emerges at higher chromium concentration due to solubility limit of the TiO_2 being exceeded, and hence the material is unable to form any crystalline phase. The anatase-to-rutile transformation is a direct result of the substitution of Ti^{4+} ions with the Cr dopant. The Cr dopant increases oxygen vacancies, subsequently reducing the strain energy in the lattice and promoting the change.[48,49] In the case of the XPS measurements of the coatings, a definitive indication as to how the Cr had been doped into the lattice was inconclusive due to no observable shift in the titanium peak. The aforementioned promotion of anatase-to-rutile transformation observed from the XRD is, however, evidence for substitutional doping of Cr in the coatings, justifying our DFT treatment of substitutional doping.[50]

The band gaps of the pure and doped coatings were compared by plotting Tauc plots, using both Ultraviolet-visible (UV-Vis) spectroscopy and ellipsometry data, as depicted in Fig. 6. A clear reduction in the band gap was observed upon doping. As the chromium concentration was increased, the

shift also became greater due to the creation of new energy levels within the band gap.

The fundamental band gap of the films was determined from the extrapolation of the linear plots of $(\alpha h\nu)^{1/2}$ vs $h\nu$ at $\alpha = 0$ for the ellipsometrically measured coatings.[32] Here, α is the absorption coefficient and is calculated from

$$\alpha = \frac{4\pi k}{\lambda}, \qquad (2)$$

where k is the extinction coefficient, λ is the wavelength, and $h\nu$ is the photon energy. The dopant band gap was calculated in a similar fashion where the extrapolation line was taken after the knee of the absorption tail. Results for all samples are detailed in Table I.

The band gap results measured for Cr-doped Cr in TiO_2 are comparable between the two sets of experimental data and also with that reported in the literature.[12–14]

The HSE06-PBEsol band gaps of pure anatase and rutile were found to be 3.25 and 3.02 eV, in good agreement with this study's experimental values and respective experimental values of about 3.2 and 3.05 eV.[51] Also, these results are in better accord with the present experimental values and those of Ref. 51 for anatase than a previous HSE06 value of 3.55 eV,[52] indicating the importance of PBEsol in conjunction with HSE06. The HSE06-PBEsol band gaps of N, C, and Cr monodoping were, respectively, 2.89, 2.84, and 2.78 eV for rutile, along with 2.95, 2.98, and 2.86 eV for anatase. A previous study[53] has suggested that the photocatalytic activity of N-doped titania under visible light results from a narrowed band gap due to overlap between N $2p$ and O $2p$ states when N concentrations are relatively high, while relatively low N concentrations result in isolated N $2p$ states just above the top of the valence band. Here, it was found that Cr and N states were present approximately 2 eV higher in energy than the tops of the respective valence bands, within the band gap; it is possible that these may act as recombination centers, particularly in the case of Cr.

The absorption spectra for pure rutile and anatase are shown in Fig. 7, as obtained from both DFT and experiment. The HSE06-PBEsol results were overlaid on the pure anatase experimental data via a cubic spline interpolation and
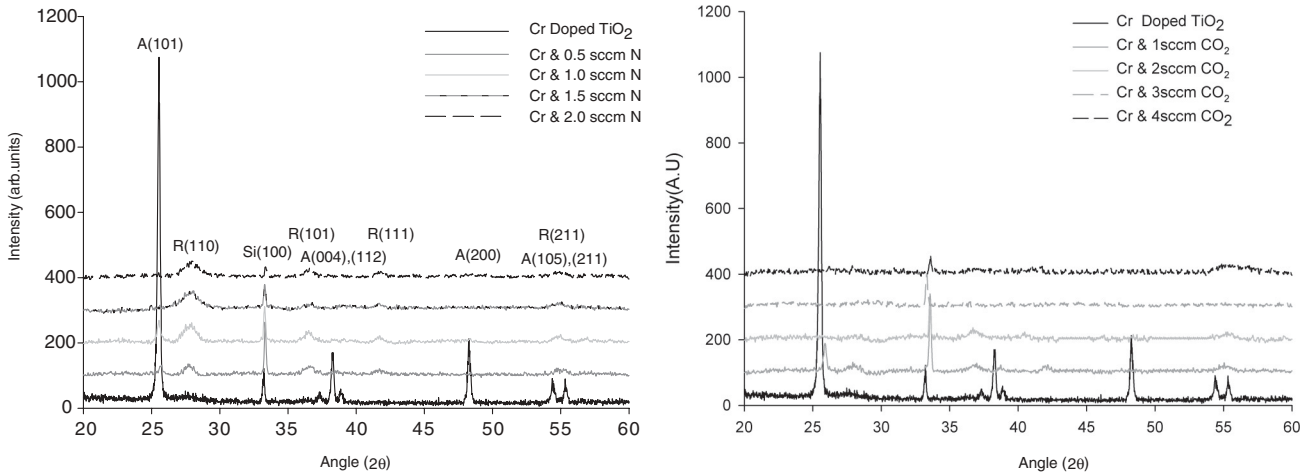
FIG. 10. XRD spectra of thermally treated Cr-N-codoped thin films with different N-dopant concentrations (left) and carbon-doped samples (right).

least-squares regression fitting procedure, with similar settings for the DFT rutile results. This study demonstrated that there was reasonably good agreement between the theoretical and experimental spectra for anatase. The corresponding spectra for Cr monodoping are depicted in Fig. 8, with similar Cr concentrations of circa 2 at.%. The experimental Cr-doped spectra at 1.8 and 2.3 at.% concentrations adopted the anatase and rutile crystal forms, respectively. These experimental data serve as a means of direct comparison with the corresponding DFT results. In Fig. 8, it can be seen that there is excellent agreement between DFT and experiment for anatase, while that for rutile shows good agreement, in semiquantitative accord. This good level of agreement between state-of-the-art DFT and experiment tends to arise largely from the use of hybrid DFT in the guise of HSE06, but also the use of the PBEsol approach to improve the optimal geometry for the solid state. However, it was found that heat treatment must be applied carefully after deposition in order to obtain consistent, good-quality absorption spectra experimentally. Therefore, it is essential to use best-practice methodology, both experimental and theoretical, to achieve optimal agreement.

Reference to Fig. 7 shows that there is an enhancement, to some extent, in the absorption spectra in the visible region upon Cr doping, by both experiment and DFT. This is consistent with the experimental and DFT results for a reduction in band gap (*vide supra*).

B. Codoping

In order to further improve the red shift of the absorption edge, anions N and C were codoped with the metallic cation Cr. The Cr concentration was set to 1.8 at% in order to ensure that the more photoactive anatase form was present. It was noted from XPS, Fig. 9, that the N was incorporated into the titania lattice in an interstitial and substitutional manner. Peaks at 399.8 eV can be ascribed to interstitial doping.[54] The substitutional atoms can be ascribed to peaks seen around 396 eV. These peaks are sometimes attributed to nitride peaks; however, the absence of nitride peaks in the XRD spectra in Fig. 10 suggest that the oxygen sites are now occupied by nitrogen-dopant atoms.[55] The other N peaks can be attributed to highly chemisorbed peaks at 397.6 eV and highly
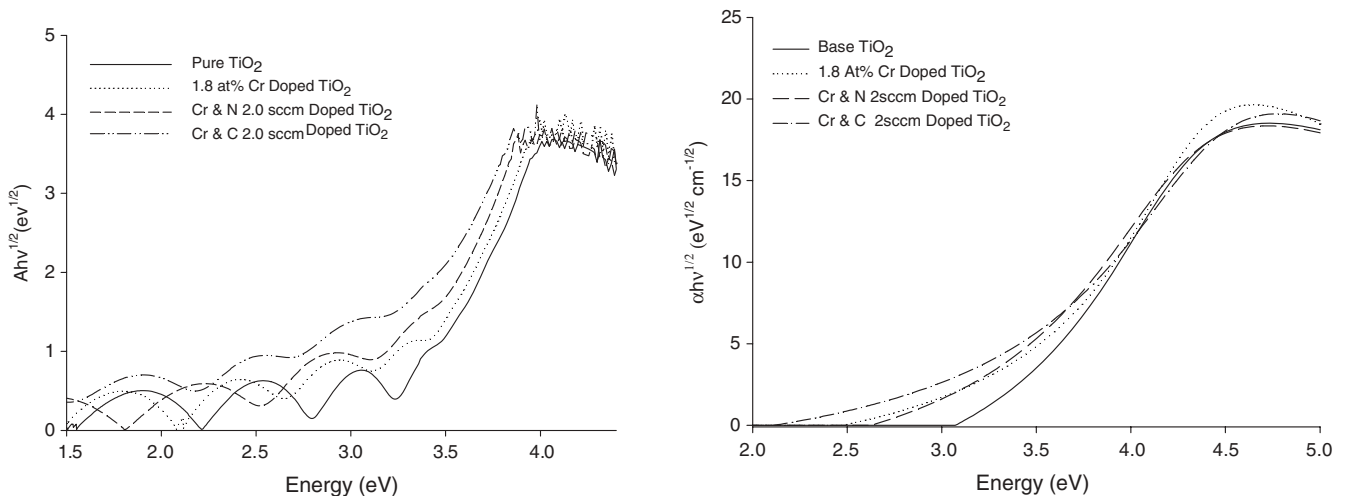

FIG. 11. Graphs of the absorbance for thermally treated Cr-monodoped and codoped samples. UV-Vis (left), ellipsometry (right).

TABLE II. Results of band gaps calculated from the Tauc plot for Cr- and N-doped samples.

N flow rate	Ellipsometry		UV-vis		Crystallite phase
	$E_{fun} +/- 0.1(eV)$	$E_{dop} +/- 0.1(eV)$	$E_{fun} +/- 0.1(eV)$	$E_{dop} +/- 0.1(eV)$	
Base TiO$_2$	3.40		3.26		Anatase
Cr 1.8 at%	3.36	2.64	3.26	3.14	Anatase
0.5 sccm	3.29	2.54	3.30	2.76	Mixed
1.0 sccm	3.22	2.66	3.27	2.72	Mixed
1.5 sccm	3.11	2.15	3.30	2.22	Rutile
2.0 sccm	3.3	2.5	3.11	2.76	Rutile

surface-confined N at 400.1 eV.[54] After thermal treatment, the XPS peaks associated with N are no longer present, except in the case of the most highly doped sample, which was deposited at a flow rate of 2 sccm. In this case, prethermal treatment XPS measurements gave an atomic concentration of 5.3%, where only 0.2 at% remains after. N is known, due to its size and method of doping to migrate about the TiO$_2$ lattice. If the N is interstitially doped, there is a tendency for it to migrate into the bulk away from the surface.[54] This migration is dependent on the duration of the heat treatment and hence the reason why it cannot be detected by the highly surface confined XPS measurements. In the case of the 2-sccm sample, it is postulated that all of dopant did not have a sufficient amount of time to migrate away from the surface. Substitutionally doped N, upon annealing, tends to react with oxygen, forming NO, which on changing to a gas phase can easily escape. An attempt was made to limit this effect by carrying out all thermal treatments in a vacuum. To investigate the carbon states present in the carbon and Cr-doped TiO$_2$, the C 1s core levels were examined by XPS. The as-deposited sample for 3 sccm of CO$_2$ shows peaks for adventitious carbon(C-C) at 284.8 eV.[56] This species of carbon was also present in the pure TiO$_2$ sample due to atmospheric contamination. Carbide carbon (Ti-C, 282.3 eV) of approximately 2 at% was also present in the as-deposited coating; this peak indicates the presence of substitutional doped carbon atoms within the coatings.[57] After thermal treatment, there are small variations in the C-C peaks; however, the Ti-C disappears completely. It has been suggested in previous papers that this loss of the Ti-C is due to its reaction with the oxygen in titania, forming volatile carbon oxide species and generating oxygen vacancies.[58] It could also be a similar situation to interstitial N explained earlier, where the C migrates into the bulk.

The XRD spectra shown in Fig. 10 indicate that the doping of N or C at small concentrations into the titania has the effect of causing rutile peaks to appear alongside its anatase counterpart. In contrast, the monodoped Cr TiO$_2$ of the same concentration showed only the anatase phase. It has been reported that a mixed phase of both anatase and rutile will show enhanced photo-activity when compared to a single phase.[59] This is considered to be a result of improved charge carrier separation due to electron trapping in the rutile phase, hence reducing electron hole recombination. As the concentrations of both N and C dopant levels are further increased, only rutile phases are observed. No characteristic peaks for titanium nitride or titanium carbide were seen in the XRD spectra, indicating that they were not formed within the coating as a separate phase.

Absorbance spectra and band gap measurements were obtained for the N and C codoped samples. Selected plots for both mono- and codoped samples are shown in Fig. 11 with a comprehensive list of the calculated band gaps shown in Tables II and III.

As previously seen for the Cr-doped titania, both experimental methods of measuring band gaps gave comparable results. Zhu *et al.* achieved a band gap of 1.5 eV with Cr-N-codoped TiO$_2$ using a sol-gel approach.[60] Although the lowest value achieved in this study was 2.15 eV for a Cr-N-codoped system, a totally different method, magnetron sputtering was used.

The HSE06-PBEsol band gaps for N/Cr and C/Cr codoping were, respectively, 2.61 and 2.55 eV for rutile, along with 2.66 and 2.59 eV for anatase. However, as would also be the case with monodoping, it should be noted that the band-edge positions are highly important, as opposed to the absolute value of the band gap itself. Other DFT studies have shown recently that Cr-C-codoped titania is not particularly suitable for hydrogen production, from consideration of band-edge

TABLE III. Results of band gaps calculated from the Tauc plot for Cr- and C-doped samples.

C flow rate	Ellipsometry		UV-vis		Crystallite phase
	$E_{fun} +/- 0.1(eV)$	$E_{dop} +/- 0.1(eV)$	$E_{fun} +/- 0.1(eV)$	$E_{dop} +/- 0.1(eV)$	
Base TiO$_2$	3.40		3.26		Anatase
Cr 1.8 at%	3.36	2.64	3.26	3.14	Anatase
1 sccm	3.26	2.64	3.31	2.99	Mixed
2 sccm	3.23	2.36	3.18	2.60	Rutile
3 sccm	3.24	2.03	3.21	2.10	Rutile
4 sccm	3.27	2.45	3.27	2.80	Rutile

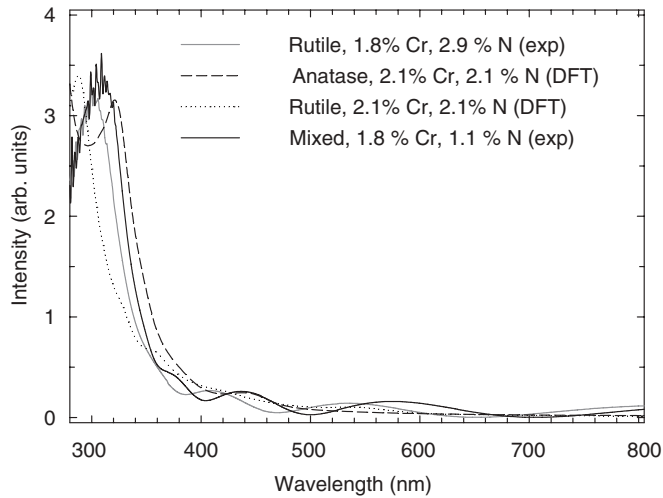FIG. 12. Absorption spectra from experiment and DFT for Cr/N-codoped titania.

FIG. 13. Absorption spectra from experiment and DFT for Cr/C-codoped titania.

positions.[29] The possible presence of recombination centers in the band gap owing to dopant states is a further factor to be borne in mind.

Absorption spectra for codoped rutile and anatase are shown in Figs. 12 (Cr/N) and 13 (Cr/C), obtained from both DFT and experiment. The experimental results correspond in (estimated) N and C concentration nearest to the approximate 2.1 at% concentration for N and C in DFT, notwithstanding previous comments as to the challenges of estimating the N and C concentrations in experiment with good accuracy. In both Cr/N and Cr/C codoping, either a mixed anatase-rutile phase is present depending on the approximate anion concentration, or alternatively rutile is formed (cf. Tables II and III)—therefore, the DFT rutile and anatase spectra are specified. It can be seen that there is reasonable agreement between anatase results from DFT and the mixed experimental results in both cases, with acceptable accord in between HSE06-PBEsol and experiment for rutile—although this could be improved. An important point to note is that Cr/C-codoped mixed phase, in particular, exhibits a visible region peak experimentally, as does the DFT anatase case (cf. Fig. 13), which is consistent with observed experimental and DFT reductions in band gap (*vide supra*).

These absorption spectra are in better agreement with experiment than our more recent treatment of doping in titania and other metal oxides, indicating the key advantage of hybrid DFT in conjunction with PBEsol for extended solids, as pointed out by Schimka *et al.*[43]

Photocurrent measurements obtained for the doped coatings show lower values when compared to those of pure TiO_2. This was a result of charge recombination within the coatings due to the incorporated dopants.

C. Formation energies

To determine the relative stability of the doped systems, the formation energy was calculated. Formation energies may be viewed as the relative difficulty for different ions to incorporate into titania and serve as a widely accepted method to gauge energetic stability. The formation energies of N, C, and N/Cr
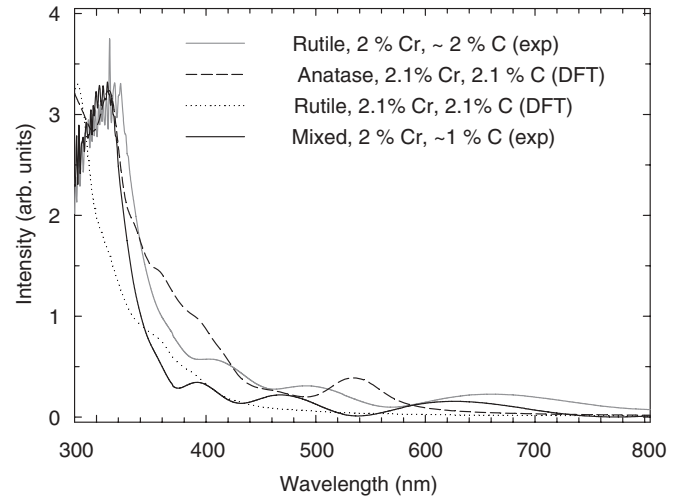
and C/Cr defects are calculated based on

$$E_{\text{form}} = E(doped) - E(pure) - \mu_{\text{NorC}}$$
$$- \mu_{\text{Cr}} + \mu_{\text{O}} + \mu_{\text{Ti}}, \qquad (3)$$

where $E(doped)$ is the total energy of the supercell containing the N, C, N/Cr, or C/Cr impurity, and $E(pure)$ denotes the total energy of the pure host TiO_2 supercell. Here, μ_{N}, μ_{C}, and μ_{Cr} are the chemical potentials of the impurities, while $\mu_{\text{O}}(\mu_{\text{Ti}})$ is the chemical potential for O (Ti). It should be noted that the formation energy depends on growth conditions, which may be varied from Ti-rich to O-rich. For TiO_2, the chemical potentials of O and Ti satisfy the relationship $\mu_{\text{Ti}} + 2\mu_{\text{O}} = \mu(TiO_2)$. O-rich growth conditions were used in this study, as this compares best to experiment; in this case, the chemical potential μ_O is determined by the energy of an O_2 molecule [$\mu_{\text{O}} = \mu(O_2)/2$], and μ_{Ti} is determined by the formula above. For N and C impurities, the chemical potentials are determined from $\mu_{\text{C}} = \mu(CO_2) - \mu(O_2)$ and $\mu_{\text{N}} = \mu(N_2)/2$. Here, μ_{Cr} is calculated from $\mu_{\text{Cr}} = \mu(Cr_2O_3)/2 - 3\mu(O_2)/4$. The formation energies are summarized in Table IV. It can be seen that (substitutional) C doping has a substantially larger formation energy than either N or Cr; this finding in terms of C vis-à-vis N mirrors our previous work.[30] This is likely due to the differences in ionic radius relative to the respective O and Ti replacement sites leading to lattice strain and serves to explain the easier experimental synthesis of N-doped titania relative to C doping.[22] Of the codoped cases, it can be seen that the anatase phase has the lower formation energy for both N/Cr and C/Cr codoping, while N/Cr codoping has a substantially lower formation energy. Therefore, the experimental viability of formation

TABLE IV. Formation energy (eV) for N-, C-, Cr- and (N, Cr)/(C, Cr)-codoped anatase/rutile.

	N	C	Cr	N-Cr	C-Cr
Rutile	4.92	12.30	0.21	4.47	12.21
Anatase	5.06	12.40	0.36	3.38	11.83

of N/Cr-codoped anatase is seen to be greatest for codoping scenarios. The 1-nn placement of the Cr in a neighboring site to the N or C is seen to reduce the formation energy relative to the respective N- or C-monodoped configurations, due primarily to a more favorable and attractive local electrostatic interaction between codopants. Of course, there is difficulty in the interpretation of the DFT formation energies, in that the dopant configurations and codopant placement may be somewhat different in experiment, given that there may not be sufficient time to reach the thermodynamically most stable 1-nn configuration (determined from DFT), or there may be some extent of interstitial doping of heterogeneity or nonuniformity in (co)dopant concentration at grain boundaries, etc. Caution is therefore advised in this respect.

IV. CONCLUSIONS

An experimental and theoretical study into mono- and codoped TiO_2 was carried out. A noticeable reduction in band gap was seen when both Cr and N/C were codoped when compared to Cr-monodoped and pure TiO_2. The crystallite phase was seen to be dependent on the amount and type of dopant incorporated into the titania. No peaks associated with chromium oxides or nitrides were observed in the XRD spectra. Both the N and C dopants were also found to be extremely mobile within the lattice upon thermal treatment. Theoretical and experimental measurements of band gaps were seen to be semiquantitatively comparable (with better agreement in some cases, particularly for anatase), indicating that theoretical calculations are becoming sufficiently mature to act as a predictive tool to accurately predict the properties of new systems with a greater level of confidence. The use of PBEsol in conjunction with HSE06 has been a key desideratum, producing band gaps and absorption spectra which are in better agreement with experiment than other GGA levels.

Photocurrent measurements obtained for the doped coatings show lower values when compared to those of pure TiO_2. This is due to charge recombination due to the dopants within the coatings. Although the photocurrent is low, potential applications for these coatings in other areas are being investigated—a key point for further study lies in a systematic variation of concentration of dopants to maximize photo-activity as a function of dopant concentration.

*Corresponding author: School of Chemical & Bioprocess Engineering, University College Dublin, Belfield, Dublin 4, Ireland; niall.english@ucd.ie

[1] A. Fujishima, Nature **238**, 37 (1972).

[2] T. Bak, J. Nowotny, M. Rekas, and C. C. Sorrell, Int. J. Hydrogen Energy **27**, 991 (2002).

[3] R. Asahi, T. Morikawa, T. Ohwaki, K. Aoki, and Y. Taga, Science **293**, 269 (2001).

[4] D. Chen, D. Yang, Q. Wang, and Z. Jiang, Ind. Eng. Chem. Res. **45**, 4110 (2006).

[5] H. Irie, Y. Watanabe, and K. Hashimoto, J. Phys. Chem. B **107**, 5483 (2003).

[6] J.-M. Herrmann, J. Disdier, and P. Pichat, Chem. Phys. Lett. **108**, 618 (1984).

[7] N. Couselo, F. S. G. Einschlag, R. J. Candal, and M. Jobbagy, J. Phys. Chem. C **112**, 1094 (2008).

[8] T. Umebayashi, T. Yamaki, H. Itoh, and K. Asai, Appl. Phys. Lett. **81**, 454 (2002).

[9] W. Y. Choi, A. Termin, and M. R. Hoffmann, J. Phys. Chem. **98**, 13669 (1994).

[10] Y. Yang, H. Wang, X. Li, and C. Wang, Mater. Lett. **63**, 331 (2009).

[11] S. Biswas, M. F. Hossain, T. Takahashi, Y. Kubota, and A. Fujishima, Phys. Status Solidi A **205**, 2023 (2008).

[12] R. Dholam, N. Patel, A. Santini, and A. Miotello, Int. J. Hydrogen Energy **35**, 9581 (2010).

[13] M. Radecka, K. Zakrzewska, M. Wierzbicka, A. Gorzkowska, and S. Komornicki, Solid State Ionics **157**, 379 (2003).

[14] C. C. Pan and J. C. S. Wu, Mater. Chem. Phys. **100**, 102 (2006).

[15] M. H. Chan, W. Y. Ho, D. Y. Wang, and F. H. Lu, Surface & Coatings Technology **202**, 962 (2007).

[16] A. Ghicov, B. Schmidt, J. Kunze, and P. Schmuki, Chem. Phys. Lett. **433**, 323 (2007).

[17] S. Sakthivel and H. Kisch, Angew. Chem., Int. Ed. **42**, 4908 (2003).

[18] S. U. M. Khan, M. Al-Shahry, and W. B. Ingler, Science **297**, 2243 (2002).

[19] T. Ohno, T. Tsubota, K. Nishijima, and Z. Miyamoto, Chem. Lett. **33**, 750 (2004).

[20] E. Barborini, A. M. Conti, I. Kholmanov, P. Piseri, A. Podestà, P. Milani, C. Cepek, O. Sakho, R. Macovez, and M. Sancrotti, Adv. Mater. **17**, 1842 (2005).

[21] J. Y. Lee, J. Park, and J. H. Cho, Appl. Phys. Lett. **87**, 011904 (2005).

[22] D. Chen, Z. Jiang, J. Geng, Q. Wang, and D. Yang, Ind. Eng. Chem. Res. **46**, 2741 (2007).

[23] Y. Gai, J. Li, S. S. Li, J. B. Xia, and S. H. Wei, Phys. Rev. Lett. **102**, 036402 (2009).

[24] W. Zhu, X. Qio, V. Iancu, X. Q. Chen, H. Pan, W. Wang, N. M. Dimitrijevic, T. Rajh, H. M. Meyer III, M. P. Paranthaman, G. M. Stocks, H. H. Weitering, B. Gu, G. Eres, and Z. Zhang, Phys. Rev. Lett. **103**, 226401 (2009).

[25]R. Dholam, N. Patel, M. Adami, and A. Miotelli, Int. J. Hydrogen Energy **33**, 6896 (2008).

[26]M. T. McCann, D. A. Mooney, M. Rahman, D. P. Dowling, and J. M. D. MacElroy, ACS Appl Mater Interfaces. **3**, 252 (2011).

[27]M. Rahman, J. M. D. MacElroy, and D. P. Dowling, J. Nanosci. Nanotech. **11**, 8642 (2011).

[28]X. Wang, S. Meng, X. Zhang, H. Wang, W. Zhong, and Q. Du, Chem. Phys. Lett. **444**, 292 (2007).

[29]R. Long, and N. J. English, J. Phys. Chem. C **113**, 8373 (2009).

[30]R. Long and N. J. English, Chem. Mater. **22**, 1616 (2010).

[31]B. von Blanckenhagen, D. Tonova, and J. Ullmann, Appl. Opt. **41**, 3137 (2002).

[32]D. Mardare, M. Tasca, M. Delibas, and G. I. Rusu, Appl. Surf. Sci. **156**, 200 (2000).

[33]S. U. M. Khan, M. Al-Shahry, and W. B. Ingler Jr, Science **297**, 2243 (2002).

[34]J. Heyd, G. E. Scuseria, and M. Ernzerhof, J. Chem. Phys. **118**, 8207 (2003).

[35]J. Paier, M. Marsman, K. Hummer, G. Kress, I. C. Gerber, and J. G. Angyan, J. Chem. Phys. **125**, 249901 (2006).

[36]J. Heyd, G. E. Scuseria, and M. Ernzerhof, J. Chem. Phys. **124**, 219906 (2006).

[37]G. Kresse and J. Hafner, Phys. Rev. B **47**, 558 (1993).

[38]G. Kresse and J. Furthermüller, Phys. Rev. B **54**, 11169 (1996).

[39]J. P. Perdew, A. Ruzsinszky, G. I. Csonka, O. A. Vydrov, G. E. Scuseria, L. A. Constantin, X. Zhou, and K. Burke, Phys. Rev. Lett. **100**, 136406 (2008).

[40]J. P. Perdew, K. Burke, and M. Ernzerhof, Phys. Rev. Lett. **77**, 3865 (1996).

[41]A. D. Becke, J. Chem. Phys. **99**, 1372 (1993).

[42]A. D. Becke, J. Chem. Phys. **99**, 5648 (1993).

[43]L. Schimka, J. Harl, and G. J. Kresse, Chem. Phys. **134**, 024116 (2011).

[44]H. J. Monkhorst and J. D. Pack, Phys. Rev. B **13**, 5188 (1976).

[45]C. J. Howard, T. M. Sabine, and F. Dickson, Acta Crystallogr. Sect. B **47**, 462 (1991).

[46]D. Chen, D. Yang, Q. Wang, and Y. Jiang, Ind. Eng. Chem. Res. **45**, 4110 (2006).

[47]J. T. Hong Zhu, Phys. Chem. C **114**, 2873 (2010).

[48]R. D. Shannon and J. A. Pask, J. Am. Ceram. Soc. **48**, 391 (1965).

[49]S. Vargas, E. Haro, and R. Rodríguez, J. Mater. Res. **14**, 3932 (1999).

[50]R. K. Sharma, M. C. Bhatnagar, and G. L. Sharma, Sensors and Actuators B: Chem. **45**, 209 (1997).

[51]Y. Zhao, C. Li, X. Liu, F. Gu, H. L. Du, and L. Shi, App. Catal. B: Environ. **79**, 208 (2008).

[52]R. Long and N. J. English, Phys. Rev. B **83**, 155209 (2011).

[53]K. Yang, Y. Dai, and B. Huang, J. Phys. Chem. C **111**, 12086 (2007).

[54]R. G. Palgrave, D. J. Payne, and R. G. Egdell, J. Mater. Chem. **19**, 8418 (2009).

[55]Z. Yang and A. Zhou, J. Wuhan University of Technol.—Mater. Sci. Ed. **22**, 457 (2007).

[56]X. Wang, S. Meng, X. Zhang, H. Wang, W. Zhong, and Q. Du, Chem. Phys. Lett. **444**, 292 (2007).

[57]F. Dong, H. Wang, and Z. Wu, J. Phys. Chem. C **113**, 16717 (2009).

[58]B. H. Q. Dang, M. Rahman, D. MacElroy, and D. P. Dowling, Surf. Coat. Technol. **205**, S235 (2011).

[59]T. Yao-Hsuan, C. S. Kuo, C. H. Huang, Y. Y. Li, P. W. Chou, C. L. Cheng, and M. S. Wong, Nanotechnology **17**, 2490 (2006).

[60]H. Zhu, J. Tao, and X. Dong, J. Phys. Chem. C **114**, 2873 (2010).